

Highly Sensitive Surface Plasmon Resonance Based D-Shaped Photonic Crystal Fiber Refractive Index Sensor

Rahul Kumar Gangwar¹ · Vinod Kumar Singh¹

Received: 5 July 2016 / Accepted: 25 September 2016 / Published online: 4 October 2016
© Springer Science+Business Media New York 2016

Abstract In this article, a D-shaped photonic crystal fiber based surface plasmon resonance sensor is proposed for refractive index sensing. Surface plasmon resonance effect between surface plasmon polariton modes and fiber core modes of the designed D-shaped photonic crystal fiber is used to measure the refractive index of the analyte. By using finite element method, the sensing properties of the proposed sensor are investigated, and a very high average sensitivity of 7700 nm/RIU with the resolution of 1.30×10^{-5} RIU is obtained for the analyte of different refractive indices varies from 1.43 to 1.46. In the proposed sensor, the analyte and coating of gold are placed on the plane surface of the photonic crystal fiber, hence there is no necessity of the filling of voids, thus it is gentle to apply and easy to use.

Keywords Photonic crystal fiber · Surface plasmon resonance · Refractive index sensor · Sensitivity

Introduction

In the last few decades, surface plasmon resonance (SPR) based sensor has attracted much attention because of its high sensitive nature and a wide range of applications. SPR based sensors have many potential applications such as biological

and chemical analyte detection, medical diagnosis, food quality control, etc. [1, 2]. Generally, SPR has been implemented in numerous sensing structures, such as prism coupling geometry, Kretschmann–Raether prism, optical waveguides, and fibers [3–6]. The prism SPR technique for the gas detection and bio sensing was first reported by Liedberg et al. in 1983 [7]. Besides Kretschmann–Raether prism performance is robust, its structural configuration is bulky and suitable for the remote sensing compare to the prism SPR technique which is simple in terms of fabrication [8, 9].

To overcome these difficulties, fiber based SPR sensors were extremely used due to its small size and low cost property [10–13]. Photonic crystal fiber (PCF) is widely used for sensing purpose, like refractive index sensor, pressure sensor, magnetic field sensor, temperature sensor, chemical and biological sensor, etc., because of its unique properties such as small size and design flexibility [14–19]. Furthermore, by optimizing the structural parameters, it is possible to enhance the sensitivity of the sensor. The main limitation of these various types of sensors is low sensitivity, where a shift in wavelength corresponds to changes in the refractive index (RI) of analyte is very small. Unlike the SPR sensor, it shows a large wavelength shift due to even small changes in RI of analyte. The first SPR sensor based on PCF was demonstrated by R. Jorgenson in 1993 [20].

Recently, Zhenkai et al. presented a RI sensor based on analyte filled PCF SPR with sensitivity of 7040 nm/RIU [21]. In such type of sensors, all the holes or metal coated hole are filled with the analyte. In all these types of SPR sensors based on PCF (solid core or hollow core), the analyte of the different refractive index needs to fill and unfilled again and again during the measurement. It is practically very difficult in real time and fast response sensing. However, filling the analyte into the air holes and coating of the metal films are also very difficult and time-consuming process. To solve above

✉ Rahul Kumar Gangwar
rahul0889@ap.ism.ac.in

Vinod Kumar Singh
singh.vk.ap@ismdhanbad.ac.in

¹ Optical Fiber Laboratory, Department of Applied Physics, Indian Institute of Technology (Indian School of Mines), Dhanbad 826004, Jharkhand, India

problem, D-shaped PCF SPR sensors have been widely used for the detection of the RI of the analyte. Nannan Laun et al. presents an SPR sensor based on D-shaped microstructured optical fiber with hollow core having sensitivity of 2900 nm/RIU [22]. A solid D-shaped fiber based on SPR sensor with the sensitivity of 7300 nm/RIU is numerically reported by Ming Tian [19].

In this paper, the sensing properties of a D-shaped PCF sensor based on SPR have been investigated by using finite element method. We have used confinement loss spectrum for determining the resonance wavelength, and systematically studied the sensitivity. The present study shows higher sensitivity of 7700 nm/RIU and a very high resolution of 1.30×10^{-5} RIU compared with previously published results [19, 23, 24]. We have also investigated the effect of the structural parameters and the thickness of the gold film on the sensing properties of the present sensor.

Design and Principle of the Proposed SPR Sensor

The cross section of the proposed D-shaped PCF with hexagonal lattice is shown in Fig. 1. Finite element method based commercial software COMSOL Multiphysics is used for the simulation. The structure has two layers of air holes. The diameter of the first air-holes layer is small as compared to the second layer hole diameter. First layer air-hole diameter is denoted by d_s , equal to $0.40 \mu\text{m}$ and the second layer hole diameter is denoted by d_l and equal to $0.80 \mu\text{m}$. The distance between two adjacent air holes is called pitch, denoted by Λ , and equal to $2.30 \mu\text{m}$ in our study. This type of D-shaped structure can be fabricated by using side polishing technique. The structure is made of silica and all the holes in the structure is empty i.e., air filled. The refractive index of the silica is determined by the Sellimeier equation.

$$n^2(\lambda) = 1 + \frac{A_1\lambda^2}{\lambda^2 - B_1} + \frac{A_2\lambda^2}{\lambda^2 - B_2} + \frac{A_3\lambda^2}{\lambda^2 - B_3} \quad (1)$$

Where λ is the wavelength, in the micrometer and Sellimeier coefficients are $A_1 = 0.696166300$, $A_2 = 0.407942600$, $A_3 = 0.897479400$, $B_1 = 4.67914826 \times 10^{-3} \mu\text{m}^2$, $B_2 = 1.35120631 \times 10^{-2} \mu\text{m}^2$, and $B_3 = 97.9340025 \mu\text{m}^2$, respectively [25]. The gold film of the thickness $t_g = 0.04 \mu\text{m}$ is deposited on the flat surface of the PCF. Johnson and Christy data [26, 27] have been used to obtain the complex dielectric constant of the gold.

Result and Discussion

We have used above optimized parameters of the proposed structure for the modal analysis. The light is propagated along

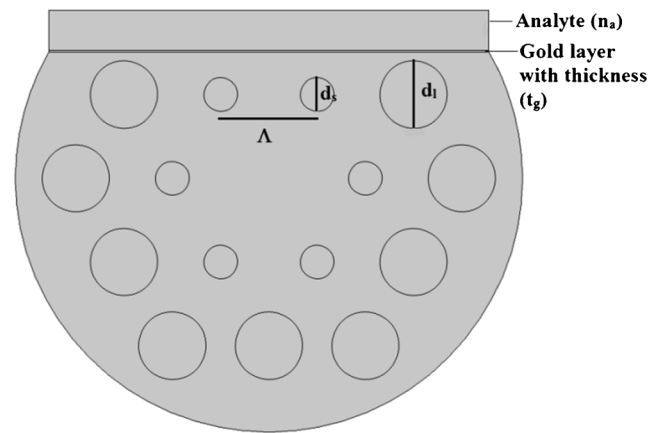


Fig. 1 Cross section of the proposed D-shaped photonic crystal fiber

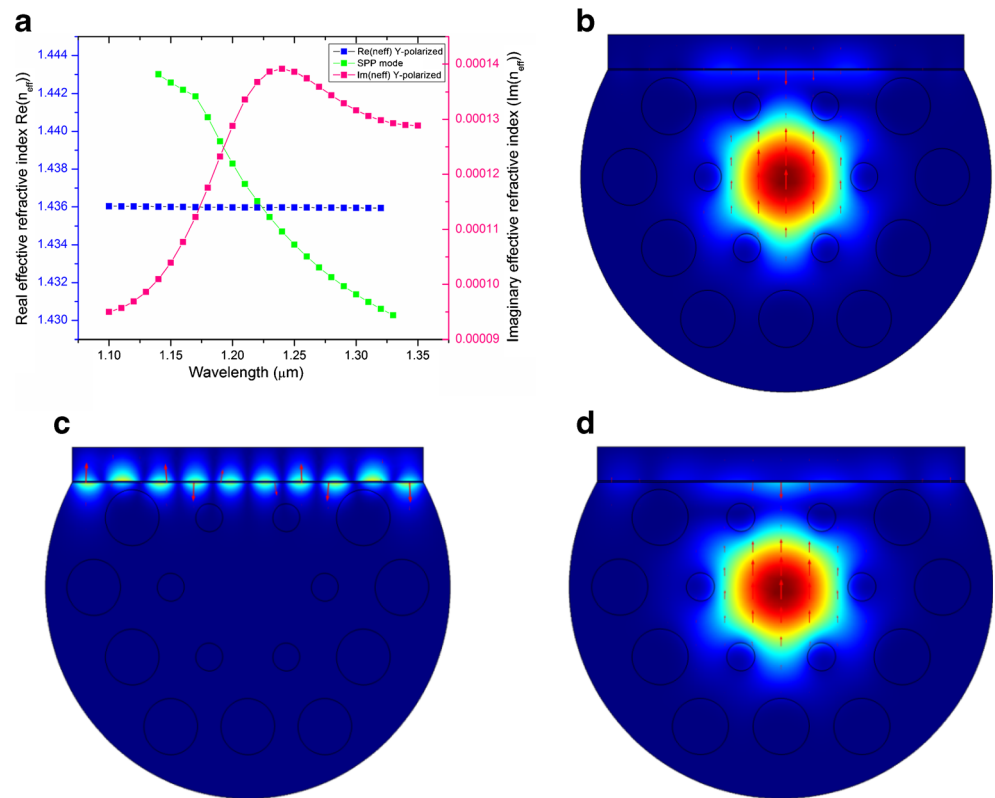
the z-direction and modal analysis is performed in the XY plane in our simulation. PCF SPR sensors are based on the surface plasmon resonance effect between surface plasmon polariton modes and the fiber core modes. It is mainly due to the evanescent fields and its interaction with the analyte. Such type of core-cladding arrangement in a line increases the leakage of the light and propagate through the core that produces more evanescent fields. This field interacts with metal layer and excites the free electrons of the metal layer easily and produces surface plasmon. At the particular wavelength, called resonance wavelength, the effective refractive index (n_{eff}) value of the core guided mode is equal to the (n_{eff}) of the surface plasmon polariton (SPP). Evanescent field easily excites the free electrons of a metal surface at the resonance wavelength which generates the surface plasmon waves (SPWs).

The propagation loss or confinement loss (α) is calculated by using the imaginary part ($\text{Im}(n_{\text{eff}})$) of the n_{eff} and is defined as [23, 25].

$$\alpha = 40\pi \cdot \frac{\text{Im}(n_{\text{eff}})}{(\ln(10)\lambda)} = 8.686 \times k_0 \cdot \text{Im}(n_{\text{eff}}) \times 10^4 \quad \text{dB/cm} \quad (2)$$

There are two fundamental mode present, namely x-polarized mode and y-polarized mode. In the proposed structure, only y-polarized fundamental mode is considered to investigate the propagation loss as x-polarized mode shows same resonance peak similar to y-polarized mode, but with lower loss depth. Figure 2 shows the resonance spectrum and the electric field distribution of the fundamental core guided mode, SPP mode, and the coupling mode at the analyte having RI $n_a = 1.44$. In Fig. 2a, the blue line shows the real part of the effective index ($\text{Re}(n_{\text{eff}})$), green line represents the SPP mode n_{eff} and pink line shows the $\text{Im}(n_{\text{eff}})$ of the y-polarized fundamental core mode. At the resonant wavelength ($1.23 \mu\text{m}$), the effective index of the core guided fundamental mode and SPP mode coincide, and at this wavelength a sharp loss peak is observed. This shows

Fig. 2 **a** Dispersion relations of the fundamental core mode (blue), plasmonic mode (green), and confinement loss spectra (pink) **b** electric field distribution of the fundamental y-polarized core mode at the wavelength 0.95 μm **c** SPP mode at the wavelength 0.95 μm , and **d** coupling mode at the resonance wavelength 1.23 μm , with the structural parameters $d_s = 0.40 \mu\text{m}$, $d_l = 0.80 \mu\text{m}$, $\Lambda = 2.30 \mu\text{m}$, and $t_g = 0.04 \mu\text{m}$



that maximum energy transfers from the core guided mode to the SPP mode at resonant wavelength.

From the Fig. 2b, it is observed that the electric field is well confined in the core region and at a metal surface for the SPP mode from Fig. 2c. In Fig. 2d, the SPP mode and fiber core mode are phase matched at wavelength 1.23 μm , and this results a sharp loss peak appears at the resonance wavelength, which is an indication of the detection of the analyte. The performance of the sensor is examined in terms of the linearity, sensitivity, and resolution.

With the help of Eq.(2), we have calculated the confinement loss of the proposed sensor for different analytes. Figure 3 shows the confinement loss spectra with analytes of different RI varies from 1.43 to 1.46, since the $\text{Re}(n_{\text{eff}})$ of the SPP mode strongly depends on the surrounding layer of the RI of the analyte. A small change in the surrounding RI of the analyte changes the $\text{Re}(n_{\text{eff}})$ of the SPP mode and also change the resonance wavelength. In Fig. 3, we have observed that as RI of the analyte increases, the resonance wavelength also increases, i.e., there is a red shift in resonance wavelength. When the RI of the analyte varies from 1.43 to 1.46 with the difference of 0.01, the resonance wavelength shifts to 0.06 μm , 0.08 μm , and 0.09 μm , respectively, towards the higher wavelength. Moreover, the confinement loss at resonance wavelength are found to be 79.20, 73.60, 56.55, and 49.06 dB/cm for the analyte of n_a equal to 1.43, 1.44, 1.45, and 1.46, respectively. As the RI of analyte is increased from

1.43 to 1.46, the effective RI of the plasmonic mode gets more and closer to the effective RI of the core-guided mode and then the mode coupling also get enhanced. This leads to a larger peak loss.

Figure 4 shows the confinement loss spectra with varying the structural parameters of the PCF and the gold thickness. In Fig. 4a, with increase in pitch (Λ) value, the loss peak shifts towards the shorter wavelength with increased confinement loss value. The minimum value of confinement loss was

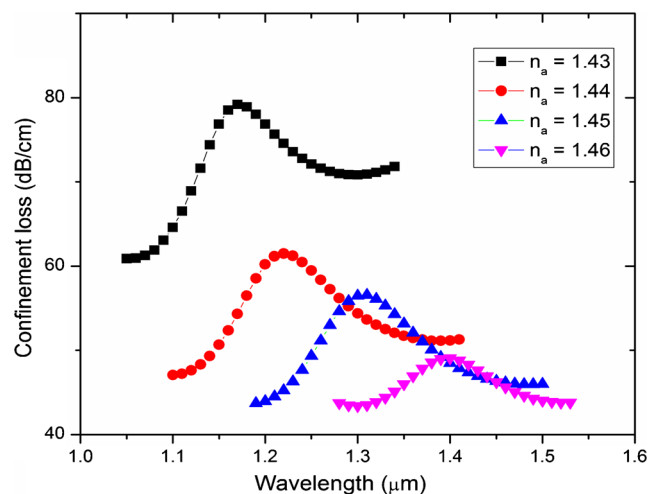


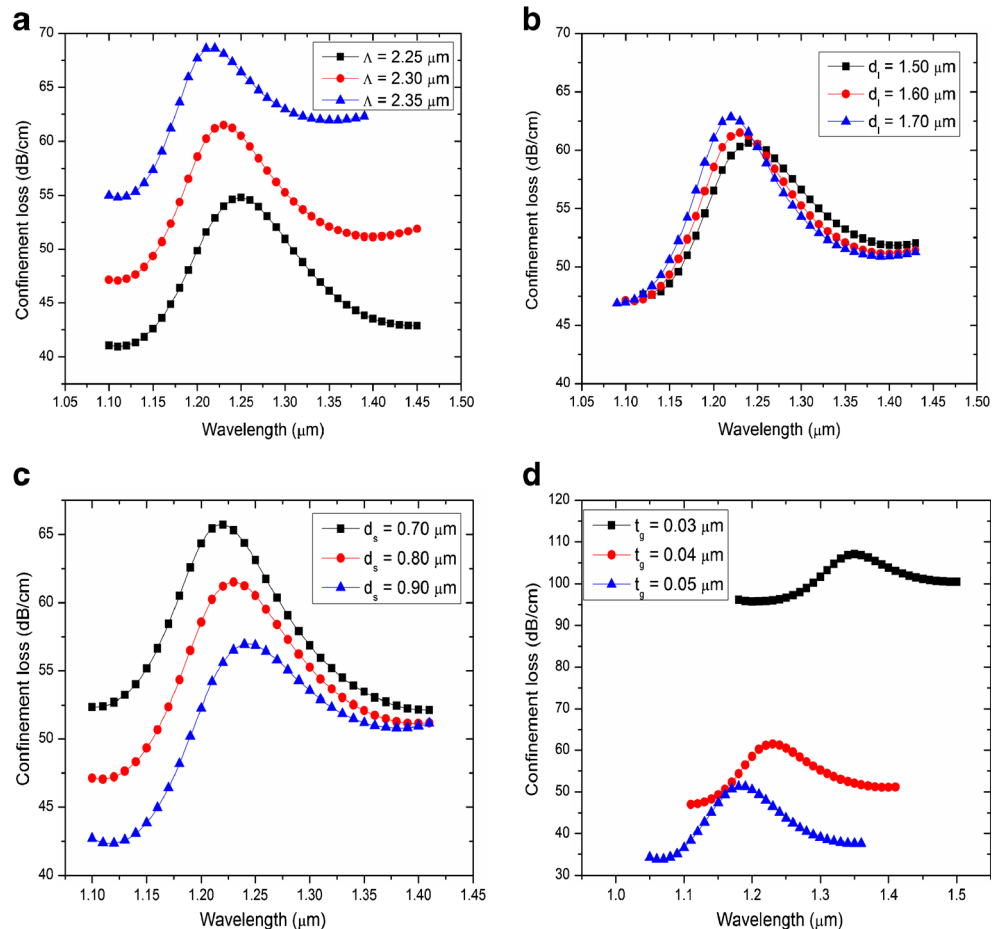
Fig. 3 Confinement loss spectrum of the proposed sensor with wavelength for analyte of different RI (n_a)

found to be 54.80 dB/cm at the resonance wavelength 1.25 μm for the pitch value of 2.25 μm where as the maximum value of confinement loss was found to be 68.23 dB/cm at the resonance wavelength 1.22 μm for the pitch value of 2.35 μm . The reason behind this is that as the pitch value is increased, the confinement of the light becomes less and less in the core region, i.e., there is a large amount of leakage of light towards the cladding region. Hence the confinement, loss is larger for higher pitch. From Fig. 4b, the loss is maximum equal to 62.83 dB/cm for the large air-hole diameter value $d_1 = 1.70 \mu\text{m}$ at the resonance wavelength 1.22 μm , and minimum 60.63 dB/cm at the wavelength 1.24 μm . In Fig. 4c, the variation of confinement loss with small air-hole diameter (d_s) is shown. Here the minimum loss is 56.93 dB/cm for the small hole diameter 0.90 μm at the resonance wavelength 1.24 μm , and maximum loss value equal to 65.70 dB/cm with $d_s = 0.70 \mu\text{m}$ at the wavelength 1.22 μm is observed. From the above study, we observed that there is a small variation in the confinement loss value by varying the large air-hole diameter compare to pitch and small air-hole diameter. As we decrease the pitch, the interaction of the y-polarized light with the metal-analyte layer interface decreases while in the case of the small air-hole diameter it is opposite. From above study,

we have obtained optimized structural parameters $d_s = 0.40 \mu\text{m}$, $d_1 = 0.80 \mu\text{m}$, $\Lambda = 2.30 \mu\text{m}$, and $t_g = 0.04 \mu\text{m}$ of the proposed D-shaped PCF for which confinement loss is minimum and wavelength shift is maximum. In this study, we have chosen small air-hole diameter for the first layer and large air-hole diameter for the second layer. This is because the small air hole helps light to leak towards the polished surface, i.e., D-shape portion and the large air hole in second layer helps to prevent the leakage of light into the cladding region. So light can leak only from the flat surface of the PCF at which gold is coated. This type of the structure helps to detect the external RI with high sensitivity.

Gold layer thickness plays an important role in the sensing performance of the sensor as well. The variation of the confinement loss with different gold thickness is shown in Fig. 4d. There is a blue shift in the resonance wavelength with increase in gold thickness. As the thickness of gold (t_g) is 0.03 μm , the maximum loss of 107.11 dB/cm is observed at the resonance wavelength of 1.35 μm , and minimum loss of 51.32 dB/cm at the wavelength 1.18 μm is calculated for the thickness of gold equal to 0.05 μm . From the graph, we have observed that the confinement loss of the sensor decreases as we increase the thickness of the gold. Due to variation of the

Fig. 4 Variation of confinement loss as a function of wavelength with varying **a** pitch (Λ) for $d_1 = 0.80 \mu\text{m}$, $d_s = 0.40 \mu\text{m}$ and $t_g = 0.04 \mu\text{m}$. **b** large air-hole diameter (d_1) for $\Lambda = 2.30 \mu\text{m}$, $d_s = 0.40 \mu\text{m}$ and $t_g = 0.04 \mu\text{m}$. **c** small air-hole diameter (d_s) for $\Lambda = 2.30 \mu\text{m}$, $d_1 = 0.80 \mu\text{m}$, and $t_g = 0.04 \mu\text{m}$, and **d** gold thickness (t_g) for $\Lambda = 2.30 \mu\text{m}$, $d_1 = 0.80 \mu\text{m}$, $d_s = 0.40 \mu\text{m}$, with $n_a = 1.44$



thickness of the gold layer, the $\text{Re}(n_{\text{eff}})$ of the SPP changes that also causes a shift in resonance wavelength. Also, the thickness of gold contributes to the lower entrance of the evanescent field towards the surface. The polariton generates at the surface of the metal near to the dielectric interface, and if we increase the thickness of the gold layer, the excited polaritons have to travel more distance to reach and interact to the analyte. Moreover, these excited polaritons have not sufficient energy to reach the metal analyte interface and interact to the analyte. Because of this reason we have chosen very carefully the optimum thickness of the gold layer to get accurate results.

Figure 5 shows the variation of the resonance wavelength with the analyte. From the Fig. 5, we observed that there is a very good linear relationship between the RI of the analyte and the resonance wavelength with linearity R^2 value equal to 0.98845 in the sensing range 1.43 to 1.46. This represents very good linear sensing response of the proposed sensor. The sensitivity of the sensor is calculated by using wavelength interrogation method from the following relation [24, 25],

$$S_\lambda = \Delta\lambda_{\text{peak}} / \Delta n_a \text{ nm/RIU} \tag{3}$$

Where $\Delta\lambda_{\text{peak}}$ is the resonance peak shift and Δn_a is the variation in the RI of the analyte.

The proposed sensor shows an average sensitivity of 7700 nm/RIU. Table 1 shows the comparison of the present work with the earlier published work. The resonance wavelengths are 1.17, 1.23, 1.31, and 1.40 μm observed for the different RI equal to 1.43, 1.44, 1.45, and 1.46, respectively. While the maximum sensitivity of 9000 nm/RIU is observed for, the analyte of RI is equal to 1.45. Most of the household liquids, e.g., kerosene oil (RI equal to 1.45), coconut oil

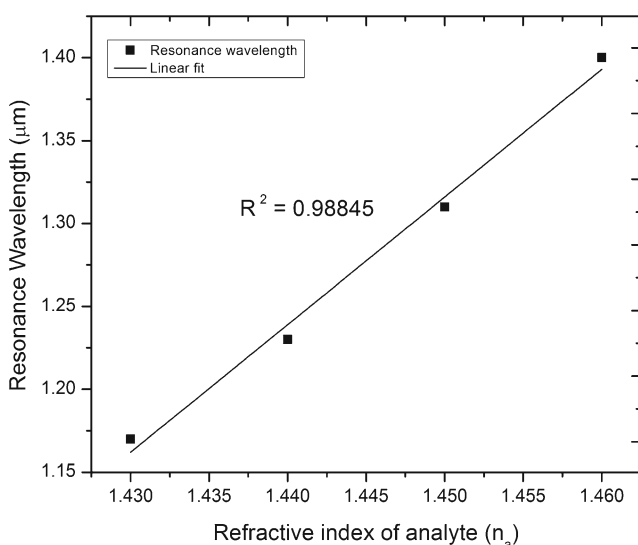


Fig. 5 Variation of resonance wavelength with analytes of different refractive index (n_a) from 1.43 to 1.46

Table 1 Comparison of sensitivity of the reported SPR sensors

Reference	Sensitivity (nm/RIU)
[19]	7300
[23]	3700
[24]	6430
Present work	7700

(1.43–1.46), olive oil (1.44–1.47), and silicon oils and some chemicals like chloroform, ethylene glycol, carbon tetrachloride etc., have a refractive index lies between 1.43–1.46. We can use the proposed sensing device to measure RI of these types of the analyte.

The resolution of the sensor is defined as,

$$R = \Delta n_a \times \frac{\Delta\lambda_{\text{min}}}{\Delta\lambda_{\text{peak}}} \text{ RIU} \tag{4}$$

Where Δn_a is the variation in the RI of the analyte, $\Delta\lambda_{\text{min}}$ is the minimum spectral resolution, and $\Delta\lambda_{\text{peak}}$ is the resonance peak shift. By considering $\Delta\lambda_{\text{min}} = 0.1 \text{ nm}$, the calculated resolution of the proposed sensor is $1.30 \times 10^{-5} \text{ RIU}$, which employs that the capability of the proposed sensor in detecting small change in RI of the analyte is of the order of 10^{-5} . Therefore, the proposed SPR based PCF sensor structure can be effectively used to measure the RI of the analyte.

Conclusion

We proposed a gold coated D-shaped PCF refractive index sensor based on SPR. The sensing properties of the proposed sensor have been calculated by using finite element method. As phase matching between the fundamental fiber core mode and the SPP mode can be encountered at the avoided crossing point, the complete resonant coupling between the fundamental mode and the SPP mode can be accomplished. The resonance wavelength can be obviously shifted with a slight change of RI of the analyte. The average sensitivity of 7700 nm/RIU and maximum sensitivity of 9000 nm/RIU are obtained with a very high resolution $1.30 \times 10^{-5} \text{ RIU}$ from the proposed sensor of the structural parameters $d_s = 0.40 \mu\text{m}$, $d_1 = 0.80 \mu\text{m}$, $\Lambda = 2.30 \mu\text{m}$ and $t_g = 0.04 \mu\text{m}$, and analytes of RI ranges from 1.43 to 1.46. Driving on the advantages of the latest nanofabrication technique, the proposed structure can be utilized for a broad scope of applications.

Acknowledgments We are thankful to IIT (ISM), Dhanbad for providing financial support. One of the authors, Rahul Kumar Gangwar also is very grateful to the Mr. Jitender, senior research fellow at IIT, Delhi for the valuable discussion.

References

- Homola J, Yee SS, Gauglitz G (1999) Surface plasmon resonance sensors: review *Sens. Actuators B Chem* 54(1–2):3–15
- Gupta BD, Verma RK (2009) Surface Plasmon resonance-based fiber optic sensors: principle, probe designs, and some applications. *Journal of Sensors* (Article ID 979761):12
- Schmidt MA, Sempere LNP, Tyagi HK, Poulton CG, Russell P, St J (2008) Waveguiding and plasmon resonances in two-dimensional photonic lattices of gold and silver nanowires. *Phys Rev B* 77(3):033417
- Skorobogatiy MA, Kabashin A (2006) Plasmon excitation by the Gaussian-like core mode of a photonic crystal waveguide. *Opt Express* 4(18):8419–8424
- Piliarik M, Homola J, Maníková Z, Čtyroký J (2003) Surface plasmon resonance sensor based on a single-mode polarization-maintaining optical fiber *Sens. Actuators B Chem.* 90(1–3):236–242
- Monzón-Hernández D, Villatoro J, Talavera D, Luna-Moreno D (2004) Optical-fiber surface-plasmon resonance sensor with multiple resonance peaks. *Appl Opt* 43(6):1216–1220
- Liedberg B, Nylander C, Lunström I (1983) Surface plasmon resonance for gas detection and biosensing *Sens. Actuators* 4:299–304
- Robinson G (1995) The commercial development of planar optical biosensors *Sens. Actuators B Chem* 29:31–36
- Hassani A, Gauvreau B, Fehri MF, Kabashin A, Skorobogatiy M (2008) Photonic crystal fiber and waveguide-based surface plasmon resonance sensors for application in the visible and near-IR. *Electromagnetics* 28(3):198–213
- Luan N, Wang R, Lu Y, Yao J (2014) Simulation of surface plasmon resonance temperature sensor based on liquid mixture-filling microstructured optical fiber. *Opt Eng* 53(6):067103
- Dash JN, Jha R (2014) Graphene-based birefringent photonic crystal fiber sensor using surface plasmon resonance *IEEE Photon Technol Lett* 26(11):1092–1095
- Liu B, Jiang Y, Zhu X, Tang X, Shi Y (2013) Hollow fiber surface plasmon resonance sensor for the detection of liquid with high refractive index. *Opt Exp* 21(26):32349–32357
- Lee K et al (2014) Refractive index sensor based on a polymer fiber directional coupler for low index sensing *opt. Exp* 22(14):17497–17507
- Gangwar RK, Bhardwaj V, Singh VK (2016) Magnetic field sensor based on selectively magnetic fluid infiltrated dual-core photonic crystal fiber. *Opt Eng* 55(2):026111–026115
- Dhara P, Singh VK (2015) Effect of MMF stub on the sensitivity of a photonic crystal fiber interferometer sensor at 1550 nm. *Opt Fiber Technol* 21:154–159
- Gangwar RK, Singh VK (2015) Refractive index sensor based on selectively liquid infiltrated dual core photonic crystal fibers. *Photonics and Nanostructures-Fundamentals and Applications* 15:46–52
- Peng Y et al (2013) Temperature sensing using the bandgap-like effect in a selectively liquid-filled photonic crystal fiber. *Opt Lett* 38:263–265
- Luan N, Wang R, Lu Y, Yao J (2014) Simulation of surface plasmon resonance temperature sensor based on liquid mixture-filling microstructured optical fiber. *Opt Eng* 53(6):067103
- Tian M, Lu P, Chen L, Lv C, Liu D (2012) All-solid D-shaped photonic fiber sensor based on surface plasmon resonance. *Opt Commun* 285(6):1550–1554
- Jorgenson R, Yee SA (1993) fiber-optic chemical sensor based on surface plasmon resonance *Sens. Actuators B Chem* 12:213–220
- Fan Z, Li S, Liu Q, An G, Chen H, Li J, Chao D, Li H, Zi J, Tian W (2015) High sensitivity of refractive index sensor based on analyte-filled photonic crystal fiber with surface plasmon resonance. *IEEE Photonics J* 7(3):1–9
- Luan N, Wang R, Lu W, Yao J (2015) Surface plasmon resonance sensor based on D-shaped microstructured optical fiber with hollow core. *Optics Express* 23(7):8576
- Dash JN, Jha R (2015) On the performance of Graphene-based D-shaped photonic crystal fibre biosensor using surface plasmon resonance. *Plasmonics* 10(5):1123–1131
- Tan Z, Li X, Chen Y, Fan P (2014) Improving the sensitivity of fiber surface plasmon resonance sensor by filling liquid in a hollow core photonic crystal fiber. *Plasmonics* 9(1):167–173
- Akowuah EK, Gorman T, Ademgil H, Haxha S, Robinson GK, Oliver JV (2012) Numerical analysis of a photonic crystal fiber for biosensing applications. *IEEE J Quantum Electron* 48(11):1403–1410
- Jitender KA, Varshney RK, Kumar M (2015) Calculation of propagation characteristics of surface plasmons in gold/silver nanowires. *Appl Opt* 54(12):715–719
- Johnson PB, Christy RW (1972) Optical constant of the noble metals. *Phys Rev B* 6:4370–4379